Published in final edited form as:
Astrophys J Lett. 2015 June 10; 806(1): . doi:10.1088/2041-8205/806/1/L3.

Discovery of SiCSi in IRC +10216: A missing link between gas and dust carriers of Si–C bonds

J. Cernicharo[1], **M. C. McCarthy**[2], **C. A. Gottlieb**[2], **M. Agúndez**[1], **L. Velilla Prieto**[1], **J. H. Baraban**[3], **P. B. Changala**[4], **M. Guélin**[5], **C. Kahane**[6], **M. A. Martin-Drumel**[2], **N. A. Patel**[2], **N. J. Reilly**[2,7], **J. F. Stanton**[8], **G. Quintana-Lacaci**[1], **S. Thorwirth**[9], and **K. H. Young**[2]

[1]Group of Molecular Astrophysics. ICMM. CSIC. C/Sor Juana Inés de La Cruz N3. E-28049, Madrid. Spain

[2]Harvard-Smithsonian Center for Astrophysics, Cambridge, MA 02138, and School of Engineering & Applied Sciences, Harvard University, Cambridge, MA 02138

[3]Department of Chemistry and Biochemistry, University of Colorado, Boulder, CO 80309

[4]JILA, National Institute of Standards and Technology and University of Colorado, and Department of Physics, University of Colorado, Boulder, CO 80309

[5]Institut de Radioastronomie Millimétrique, 300 rue de la Piscine, F-38406, St-Martin d'Hères, France

[6]Universit Grenoble Alpes, IPAG, F-38000 Grenoble, France; CNRS, IPAG, F-38000 Grenoble, France

[8]Institute for Theoretical Chemistry, Department of Chemistry, The University of Texas at Austin, Austin, TX 78712

[9]I. Physikalisches Institut, Universität zu Köln, Zülpicher Str. 77, 50937 Köln, Germany

Abstract

We report the discovery in space of a disilicon species, SiCSi, from observations between 80 and 350 GHz with the IRAM[10] 30m radio telescope. Owing to the close coordination between laboratory experiments and astrophysics, 112 lines have now been detected in the carbon-rich star CW Leo. The derived frequencies yield improved rotational and centrifugal distortion constants up to sixth order. From the line profiles and interferometric maps with the Submillimeter Array[11], the bulk of the SiCSi emission arises from a region of 6″ in radius. The derived abundance is comparable to that of SiC_2. As expected from chemical equilibrium calculations, SiCSi and SiC_2 are the most abundant species harboring a Si–C bond in the dust formation zone and certainly both play a key role in the formation of SiC dust grains.

[10]This work was based on observations carried out with the IRAM 30-meter telescope. IRAM is supported by INSU/CNRS (France), MPG (Germany) and IGN (Spain)

[11]The Submillimeter Array is a joint project between the Smithsonian Astrophysical Observatory and the Academia Sinica Institute of Astronomy and Astrophysics, and is funded by the Smithsonian Institution and the Academia Sinica.

[7]Present address: Department of Chemistry, Marquette University, Milwaukee, WI 53233

Europe PMC Funders Author Manuscripts

Keywords

Stars: individual (IRC+10216); stars: carbon; astrochemistry; stars: AGB and post-AGB

1. Introduction

Interstellar dust grains are synthesized in two main types of sources: the inner winds of asymptotic giant branch (AGB) stars and the ejecta of massive stars, mainly supernovae (SNe). Dust grains are formed from molecular seeds. In AGB stars, molecules such as TiO, VO, ZrO, C_2, CN, and C_3, among others, are known to be present in their photospheres since the beginning of the 20th century. Because of the high stability of the CO molecule, depending on whether the C/O ratio is >1 (C stars) or <1 (M stars), the gas becomes either carbon- or oxygen-rich after CO reaches its equilibrium abundance, leading to a different chemistry and therefore to different dust formation schemes. In SNe, different types of dust can be formed depending on the degree of enrichment in heavy elements. The dust formation effciency in SNe is still a matter of debate. Recent studies with the *Herschel* Space Telescope point to much larger dust masses than previously thought (Matsuura et al. 2011, 2015).

Dust formation can be simplified as a two-step process: formation of nucleation seeds followed by grain growth through condensation of refractory molecules at high temperature and other less refractory species at larger distances from the star. There are, however, many mysteries in this picture of events, starting from the fundamental step of the formation of the nucleation seeds, which essentially are refractory species (Gail 2010). The presence of SiC grains in C-rich AGBs was confirmed by the detection of an emission band at ~11.3 μm (Treffers & Cohen 1974). This band has been found towards a large number of C-rich stars with the IRAS and ISO satellites. However, the molecular precursors of SiC dust grains are still unknown. SiC molecules have been detected in the external shells (≥300 R_*) of IRC +10216 (Cernicharo et al. 1989; Patel et al. 2013). In the inner layers, the most abundant molecule harbouring a Si–C bond is SiC_2 (Thaddeus et al. 1984; Cernicharo et al. 2010), whereas the most abundant Si-bearing species is SiS, which, together with SiO and SiC_2, account for a significant fraction of the available silicon (Agúndez et al. 2012).

CW Leo, located ≃130 pc from us, is a Mira variable star with a period of 630-670 days and an amplitude of ≃1 mag in the *K* band (Menten et al. 2012). It is one of the brightest infrared sources in the sky. Due to its close proximity, IRC +10216, the circumstellar envelope of CW Leo, has attracted many studies because it is exceptionally rich in molecular species. Half of the known interstellar species are observed in this C-rich envelope. The observed molecules range from CO, the main tracer of the cool molecular gas, and other diatomic and triatomic species (see e.g. Cernicharo et al. 2000, 2010), to molecules containing refractory elements (Cernicharo & Guélin 1987), and long carbon chain species C_nH and their anions (Cernicharo & Guélin 1996; Cernicharo et al. 2008; Guélin et al. 1997; McCarthy et al. 2006; Thaddeus et al. 2008, and references therein). Among the species detected in this source, the silicon-carbon species Si_nC_m could play an important role as seeds of SiC dust grains. The simplest members of such a family, SiC

(Cernicharo et al. 1989), and SiC_2 (Thaddeus et al. 1984), are known to be present in IRC +10216. However, Si_2C (hereafter SiCSi), which is predicted to be very abundant from chemical equilibrium calculations (Tejero & Cernicharo 1991; Yasuda & Kozasa 2012) and could play a key role in the formation of SiC dust grains, has not been found so far.

In this Letter we present the detection of SiCSi in IRC +10216 based on a close coordination between laboratory, astrophysics and radio astronomy. This synergy has resulted in the detection of 112 lines of this new species using data from the IRAM 30-m radio telescope. Nine of these lines are also detected with the Submillimeter Array (SMA).

2. Observations

In the course of searches for new molecules we have covered a large fraction of the 3, 2, 1 and 0.8 mm spectrum of IRC+10216 with a high sensitivity using the 30-m IRAM radio telescope. In the 3 mm window, the data acquired during the last 30 years cover the 80-116 GHz domain with very high sensitivity (1-3 mK). Examples of these data can be found in Agúndez et al. (2008, 2014), Cernicharo & Guélin (1996), Cernicharo et al. (2007, 2008), and references therein. Most of the 2 mm data come from the line survey of IRC +10216 carried out by Cernicharo et al. (2000), complemented with additional data obtained during the search for specific molecular species (see, e.g. Guélin et al. 2004; Agúndez et al. 2008, 2012; Fonfría et al. 2006). The sensitivity of the 2 mm observations varies between 1.5 and 10 mK. The 1 mm and 0.8 mm data come from observations carried out during the searches quoted above and a line survey between 290 and 355 GHz carried out using the new EMIR receivers in 2010 and 2011 with a sensitivity of 2-5 mK, depending on the atmospheric transmission.

For frequencies above 250 GHz the spectrometers were two autocorrelators with 2 MHz of spectral resolution and 4 GHz of bandwidth. For all other observations the spectral resolution was 1 MHz provided by filter banks or autocorrelators. The observing mode, in which we wobbled the secondary mirror by ±90" at a rate of 0.5 Hz, and the dry weather conditions (sky opacity at 225 GHz was below 0.1 in most observations) ensured flat baselines and low system noise temperatures ($T_{sys} \simeq$ 100-400 K depending on the frequency).

The selected observing method, with the off position located at 180″ from the star, provides reference data free from emission for all molecular species but CO (see Cernicharo et al. 2015). The emission of all other molecular species is restricted to a region ≤ 20-30″ (see, e.g., Guélin et al. 1993). The intensity scale, antenna temperature (T_A^*), was corrected for atmospheric absorption using the ATM package (Cernicharo 1985; Pardo et al. 2001). The main beam antenna temperature can be obtained by dividing T_A^* by the main beam effciency of the telescope which is 0.81, 0.59, and 0.35 at 86, 230, and 340 GHz, respectively. Calibration uncertainties for data covering such a large observing period have been adopted to be 10%, 15%, 20%, and 30% at 3, 2, 1, and 0.8 mm, respectively. Additional uncertainties could arise from the line intensity fluctuation with time induced by the variation of the stellar infrared flux, which has been recently discovered by Cernicharo et al. (2014). All data have been analyzed using the GILDAS package[1].

The data revealed several hundreds of spectral lines which could not be assigned to any known molecular species collected in the public CDMS (Müller et al. 2005) and JPL (Pickett 1998) spectral databases and in the MADEX code (Cernicharo 2012). Most of these lines show the characteristic U-shaped or flatted profiles with linewidths of 29 km s^{-1}. However, above 250 GHz a significant number of lines are very narrow and come from the dust formation zone of CW Leo (see, e.g., Patel et al. 2011; Cernicharo et al. 2013). Among the unidentified lines observed with the IRAM 30-m telescope, we have been able to assign 112 to the rotational spectrum of SiCSi through an iterative procedure described below and a close synergy between molecular spectroscopy and astrophysics. Some selected lines among those observed in IRC +10216 are shown in Figure 1. Nine lines observed above 300 GHz with the IRAM 30-m telescopes and assigned to SiCSi correspond to unidentified lines observed with the SMA by Patel et al. (2011). The spatial distribution of some of these lines, as derived with the SMA, is shown in Figure 2.

3. Spectroscopic constants of SiCSi

Disilicon carbide (SiCSi) has a C_{2v} symmetry and a $^1A_1$ electronic ground state with a modest permanent dipole moment of ~1 D along the *b*-inertial axis (Gabriel et al. 1992; Barone et al. 1992; Bolton et al. 1992; Spielfiedel et al. 1996; McCarthy et al. 2015). Because the two equivalent off - axis silicon atoms are bosons, only half of the rotational levels exist ($K_a + K_c$ even).

The search for lines of SiCSi in space began with the lines measured in the laboratory by McCarthy et al. (2015), which allowed us to accurately predict frequencies with $K_a = 0, 1$ in the 3 mm domain. Although the molecule is predicted to be rather floppy, with deviations up to 10-20 MHz for transitions higher in J than those measured in the laboratory ($J \leq 10$), we quickly found 3 lines in the 3 mm spectrum of IRC +10216 that could be analyzed simultaneously with the laboratory lines. From the newly derived spectroscopic constants, which now include additional centrifugal distortion terms, we searched for additional lines until we found all the intense lines predicted in the 3 mm domain with upper level energies below 100 K. Using the spectroscopic constants derived from a combined fit to the laboratory and IRC +10216 data, we continued the search for $K_a = 0, 1$ lines in the 2 mm and 1 mm domains, and up to 20 additional lines were easily identified. Differences between the predicted and observed frequencies were again 10-50 MHz, but because the lines are so intense (typically 10-20 mK) and have a distinctive line shape, it was not diffcult to make additional assignments (see Figure 1). Nevertheless, on occasion, we had to discard several initial assignments because subsequent predictions failed to predict new lines. With the laboratory lines and the ~30 astronomical lines involving $K_a = 0$ and 1 levels, a refined set of constants were derived, and we then proceeded to search for lines with $K_a = 2, 3$ in the entire 30 m data set of IRC +10216 that was available to us. With these new astronomical measurements in hand, several additional lines with frequencies up to 180 GHz were measured in the laboratory. Most importantly, several of these lines correspond to transitions involving $K_a = 1$ and 2 levels, which enabled us to precisely determine the D_K term, and confirm the astronomical assignments with higher K_a.

[1] http://www.iram.fr/IRAMFR/GILDAS

Ultimately, we were able to assign 112 lines in IRC +10216 to SiCSi with $J \leq 48$ and $K_a \leq 5$. At least 30% are free of blending, and the uncertainties of the derived frequencies are less than 1 MHz. Other lines were slightly blended, but from their characteristic line profile it was still possible to measure their frequencies with an accuracy of ~1 MHz. Above 250 GHz, most observations have a spectral resolution of 2 MHz and the frequencies are accurate to 1-1.5 MHz. From the unblended lines, an average expansion velocity of 14.0±1.0 km s^{-1} was derived, which is similar to that obtained for most lines in IRC +10216 (Cernicharo et al. 2000). Hence, the discovery of SiCSi in IRC +10216 –which is based on 112 observed lines– is one of the most robust identifications ever published for a first detection of a molecule in space. Some 20 additional lines have been also identified, but they are so heavily blended that accurate frequencies and intensities could not be derived.

The rotational constants were derived with a Watson Hamiltonian that included distortion constants up to sixth order in the *A* and *S* reductions (Table 1). The fit with the *S* reduction was done with the SPFIT program Pickett (1991), while that in the *A* reduction was done with fitting programs associated with MADEX (Cernicharo 2012). We confirmed that both SPFIT and MADEX yielded the same results in the *A* reduction. The rotational constants in the *A* and *S* reductions agree rather well, but the *S* reduction is preferred because δ_K and h_{JK} are three orders of magnitude larger than the corresponding constants d_1 and h_2 and the predicted frequencies for high *J* or K_a will be less accurate. Because there are only a few observed lines with $K_a > 3$, further improvement of the rotational constants was not possible. We estimate that the calculated frequencies with $J \leq 60$, $K_a \leq 5$ are reliable up to 400 GHz. The list of observed lines in IRC +10216, together with the derived line parameters, energies of the upper levels, and line strengths is provided in Table 2 (online), which also gives the frequencies and uncertainties for the 22 lines observed in the laboratory (McCarthy et al. 2015).

The SiCSi distortion constants are as large as those of SiC_2, a well-studied molecule also considered to be very floppy. Table 1 provides, for comparison purposes, the rotational constants derived from a fit to the lines of SiC_2 reported by Müller et al. (2012) including the same constants as for SiCSi plus additional higher distortion constants. Both, Δ_K and H_K are one order of magnitude larger for SiCSi than for SiC_2, while Δ_{JK} and H_K are of the same order despite SiCSi being somewhat heavier than SiC_2. Both molecules have a very low-lying vibrational mode, around 100-200 cm^{-1}. Hence, by analogy with SiC_2 for which the antisymmetric ν_3 mode is readily observed in IRC +10216, we might also expect to observe rotational lines of SiCSi in its symmetric mode ν_2. Nevertheless, SiCSi has its dipole moment along the *b*-axis while in SiC_2 it is aligned along the *a*-axis which produce a significantly different rotational spectrum.

4. Discussion

The observed line profiles of SiCSi go from U-shaped, in the case of low excitation lines lying at high frequencies and thus observed with a smaller beam, to flat-topped, for high-excitation lines lying at low frequencies (see Figure 1). Such behaviour indicates that SiCSi is concentrated around the star but with a relatively extended distribution, as occurs in the case of metal-bearing species (Cernicharo & Guélin 1987; Guélin et al. 1993). The SMA

maps, which correspond to transitions involving upper level energies between ~60 and ~100 K, show that the emission is concentrated in a region of $\simeq 6''$ in diameter (see Figure 2). A slightly larger brightness distribution size can be expected for lines involving lower energy levels (see Figure 1). We have checked if SiCSi could be responsible for some of the lines detected with ALMA in IRC +10216 (Cernicharo et al. 2013). Unfortunately, only three strong lines are within the spectral domain covered by these ALMA cycle0 observations and only one seems to be free of blending and is clearly detected in the central pixel. However, these observations were selected to trace the dust formation zone and their sensitivity is not good enough to trace the spatial distribution of weak lines.

To initially estimate the abundance and origin of the SiCSi emission from transitions involving different energies, we show in the top panel of Figure 3 a rotational diagram based on the 112 observed lines. We have adopted a gaussian source size with a radius $5''$. The observed integrated intensities have been corrected for dilution in the beam and for the main beam effciency of the telescope. We can distinguish three zones with different rotational temperatures. The lines with upper level energies below 60 K (zone I) have been fit with a rotational temperature, T_{rot}, of 31 ± 5 K and a column density of (1.4 ± 0.4) × 10^{15} cm^{-2}. The lines with upper level energies between 60 and 200 K (zone II) have been fit with T_{rot} = 118 ± 12 K and a column density of (3 ± 0.7) × 10^{15} cm^{-2}. Finally, the lines with upper level energies above 200 K (zone III) have been fit with T_{rot} = 280 ± 50 K and a column density of (3.2 ± 0.9) × 10^{15} cm^{-2}. The rotational temperature derived for zone I could correspond well with the extended molecular ring observed at $r \simeq 14''$ in SiC_2 (Guélin et al. 1993). Its value agrees well with the rotational temperature derived for other species (Agéndez et al. 2008; Cernicharo & Guélin 1996). Zone II corresponds to the emission region of metal-bearing species and high energy lines of SiC_2 with $r \leq 5''$ (Figure 2 and Velilla Prieto et al. 2015). Finally, the high energy lines (zone III) correspond to the region with $r \leq 2''$ traced by high-J lines and vibrationally excited states of SiC_2, SiS, HCN, HNC among other species (Cernicharo et al. 2010, 2011; Velilla Prieto et al. 2015). In this region, Cernicharo et al. (2010) derived for SiC_2 $T_{rot} \simeq 204$ K and a column density of ~ 8 × 10^{13} cm^{-2} averaged over a beam of $30''$. When corrected for the source radius of $5''$ adopted in this work, the column density of SiC_2 becomes 3 × 10^{15} cm^{-2}. Hence, SiCSi is as abundant as SiC_2 in the dust formation zone of IRC +10216. The large difference in the intensities of the observed lines of SiCSi and SiC_2, near a factor of 100, arise from the lower dipole moment and the larger partition function of SiCSi. When corrected for these e ects, the observed intensities of the individual lines of SiCSi and SiC_2 indicate a SiC_2/SiCSi abundance ratio of about 5.

Early chemical equilibrium calculations by Tejero & Cernicharo (1991) showed that in the inner envelope of C-rich AGB stars the most abundant gas phase species containing a Si–C bond are SiC_2 and SiCSi, while SiC is predicted to be present with a much lower abundance (see also Yasuda & Kozasa 2012 and Figure 3). To constrain the abundance and spatial distribution of SiCSi in IRC +10216 we have carried out radiative transfer calculations to obtain the emergent line profiles and compare them with the observed ones. The physical model of the envelope is taken from Agúndez et al. (2012) with the downward revision of the density of particles in the regions inner to 5 R_* derived by Cernicharo et al. (2013). Since

collisional rate coeffcients are not available for SiCSi we have assumed local thermodynamic equilibrium, which is a reasonable approximation given the low dipole moment of SiCSi. We find that the intensities and profiles of the low excitation lines observed can be well reproduced by adopting a SiCSi abundance relative to H_2 of 4×10^{-8}, from the inner layers out to the photodissociation region. We have assumed that SiCSi is photodissociated by the ambient interstellar ultraviolet field with a rate of $10^{-9} \times \exp(-2A_V)$ s^{-1}, where A_V is the visual extinction. However, to reproduce the high intensities observed for lines involving upper level energies above 200 K, it is necessary to increase the abundance of SiCSi in the warm inner regions to 2×10^{-7} (see Figure 3). Finally, a depletion in the very inner regions, which is consistent with the expectations from chemical equilibrium, yields a better agreement with the observed line profiles (see Figure 1). The derived abundance profile for SiCSi is shown in Figure 3.

High angular resolution interferometric observations are needed to better constrain the abundance gradient of SiCSi in the inner layers. In any case, we find that disilicon carbide is as abundant as silicon dicarbide in the inner layers. The depletion in the abundance of SiCSi at 50 R_*, which leads to a SiC_2/SiCSi abundance ratio of $\simeq$5 in the outer regions, would be consistent with its incorporation into SiC dust grains.

Acknowledgments

We thank spanish MINECO for funding under grants AYA2009-07304, AYA2012-32032, CSD2009-00038, and ERC under ERC-2013-SyG, G.A. 610256 NANOCOSMOS. The new laboratory measurements in Cambridge were supported by NASA Grant NNX13AE59G.

REFERENCES

Agúndez M, Cernicharo J, Guélin M. ApJ. 2007; 662:L91.
Agúndez M, Fonfría JP, Cernicharo J, et al. A&A. 2008; 479:493.
Agúndez M, Cernicharo J, Guélin M, et al. A&A. 2010; 517:L2.
Agúndez M, Fonfría JP, Cernicharo J, et al. A&A. 2012; 543:A48.
Agúndez M, Cernicharo J, Guélin M. A&A. 2014; 570:45.
Barone V, Jensen P, Minichino C. J. Mol. Spectrosc. 1992; 154:252.
Bolton EE, DeLeeuw BJ, Fowler JE, et al. J. Chem. Phys. 1992; 97:5586.
Cernicharo, J. Internal IRAM report. IRAM; Granada: 1985.
Cernicharo J, Guélin M. A&A. 1987; 183:L10.
Cernicharo J, Gottlieb CA, Guélin, et al. ApJ. 1989; 341:L25.
Cernicharo J, Guélin. A&A. 1996a; 309:127.
Cernicharo J, Guélin M, Kahane C. A&AS. 2000; 142:181.
Cernicharo J, Guélin M, Agúndez M, et al. A&A. 2007; 467:L37.
Cernicharo J, Guélin M, Agúndez M, et al. ApJ. 2008; 688:L83.
Cernicharo J, Waters LBFM, Decin L, et al. A&A. 2010; 521:L8.
Cernicharo J, Agúndez M, Kahane C, et al. A&A. 2011; 529:3.
Cernicharo, J. ECLA-2011: Proc. of the European Conference on Laboratory Astrophysics. Stehl, C.; Joblin, C.; d'Hendecourt, L., editors. Cambridge Univ. Press; Cambridge: 2012. p. 251 EAS Publications Series 2012
Cernicharo J, Daniel F, Castro-Carrizo A, et al. ApJ. 2013; 778:L25.
Cernicharo J, Teyssier D, Quintana-Lacaci G, et al. ApJ. 2014; 796:L21.
Cernicharo J, Marcelino N, Agúndez M, Guélin M. A&A. 2015; 575:A91.

Fonfría JP, Agúndenz M, Pardo JR, et al. ApJ. 2006; 646:L127.
Gabriel W, Chambaud G, Rosmus P, et al. ApJ. 1992; 398:706.
Gail HP. Lect. Notes Phys. 2010; 815:61.
Guélin M, Lucas R, Cernicharo J. A&A. 1993; 280:L19.
Guélin M, Cernicharo J, Travers MJ, et al. A&A. 1997; 317:L1.
Guélin S, Muller, Cernicharo J, et al. A&A. 2004; 426:L49.
Matsuura M, Dwek E, Meixner M, et al. Science. 2011; 333:1258. [PubMed: 21737700]
Matsuura M, Dwek E, Barlow M, et al. ApJ. 2015; 800:50.
McCarthy MC, Gottlieb CA, Gupta H, Thaddeus P. ApJ. 2006; 652:L141.
McCarthy M, et al. J. Phys. Chem. Lett. 2015 submitted.
Menten KM, Reid MJ, Kaminski T, Claussen MJ. A&A. 2012; 543:A73.
Müller HSP, Schlöder F, Stutzki J, Winnewisser G. J. Mol. Struct. 2005; 742:215.
Müller HSP, Cernicharo J, Agúndez M, et al. J. Mol. Spectrosc. 2012; 271:50.
Pardo JR, Cernicharo J, Serabyn E. IEEE Trans. Antennas and Propagation. 2001; 49:12.
Patel NA, Young KH, Gottlieb CA, et al. ApJS. 2011; 193:17.
Patel, NA.; Gottlieb, CA.; Young, KH. The Life Cycle of Dust in the Universe: Observations, Theory, and Laboratory Experiments - LCDU 2013. Taipei, Taiwan: 2013.
Pickett HM. J. Mol. Spectrosc. 1991; 148:371.
Pickett HM, Poynter RL, Cohen EA, et al. J. Quant. Spectrosc. Radiat. Transfer. 1998; 60:883.
Spielfiedel A, Carter S, Feautrier N, et al. J. Phys. Chem. 1996; 100:10055.
Tejero, J.; Cernicharo, J. Modelos de Equilibrio Termodinaámico Aplicados a Envolturas Circunestelares de Estrellas Evolucionadas. IGN; Madrid: 1991.
Thaddeus P, Cummins SE, Linke RA. ApJ. 1984; 283:L45.
Thaddeus P, Gottlieb CA, Gupta H, et al. ApJ. 2008; 677:1132.
Treffers R, Cohen M. ApJ. 1974; 188:545.
Velilla Prieto L, et al. submitted to ApJ Letters. 2015
Yasuda Y, Kozasa T. ApJ. 2012; 745:159.

Europe PMC Funders Author Manuscripts

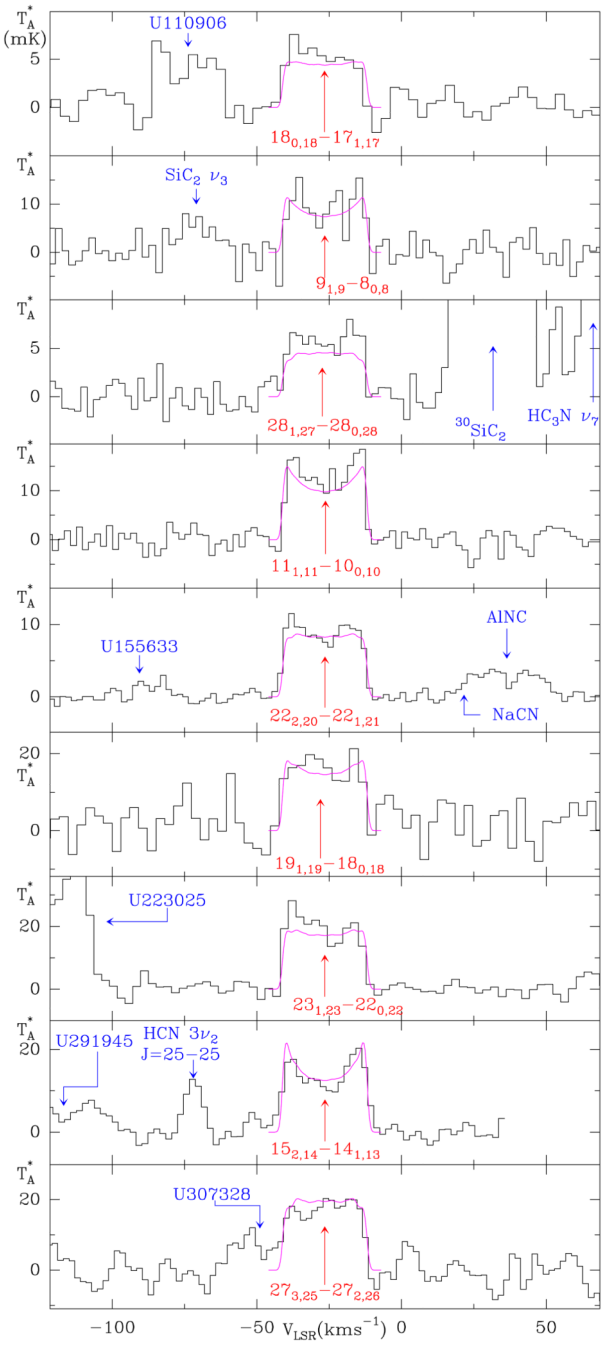

Fig. 1.

Selected transitions of SiCSi among the 112 observed lines. Unidentified (U) lines are indicated by their frequency in MHz. The intensity scale is antenna temperature in mK. The data are shown as histograms. Violet continuum lines show the predicted line profile from the best model for the abundance of SiCSi (see text).

Europe PMC Funders Author Manuscripts

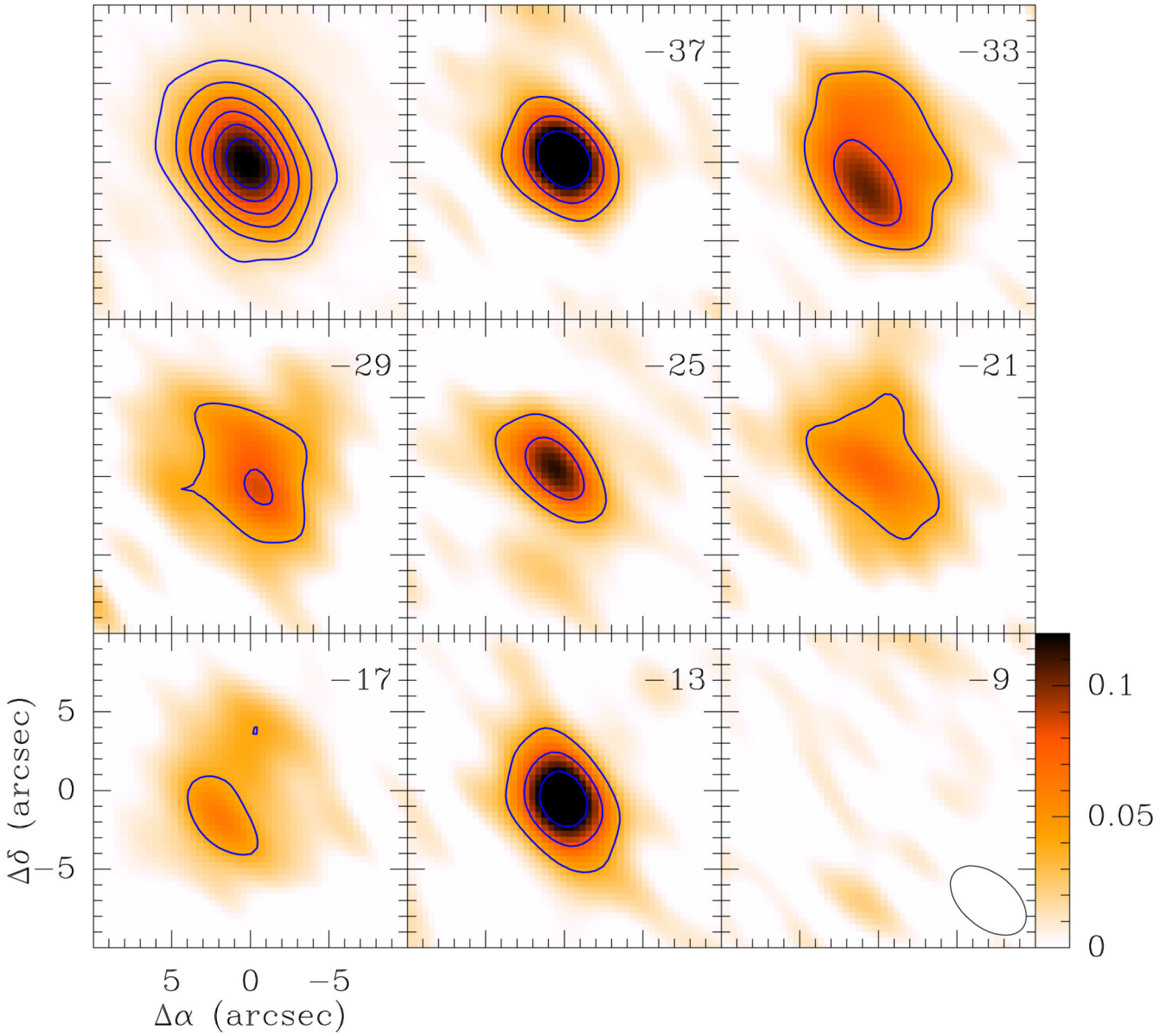

Fig. 2.

Maps of the average of four SiCSi lines: $18_{3,15} - 18_{2,16}$, $16_{3,13} - 16_{2,14}$, $14_{3,11} - 14_{2,12}$ and $12_{3,9} - 12_{2,10}$ (from the SMA line survey of IRC +10216 Patel et al. (2011)). Their visibilities were combined before imaging. The upper left panel is the integrated intensity map, while the remaining ones are the channel maps with V_{LSR} velocities indicated on top right in km s^{-1}. The size of the synthesized beam is shown in bottom right panel. The halftone image in the first panel is scaled linearly from 0 to 2.7 Jy $beam^{-1}$ km s^{-1} and the contour levels (in the same units) have the starting value and intervals of 0.4 in the first panel and 0.04 in remaining panels.

Europe PMC Funders Author Manuscripts

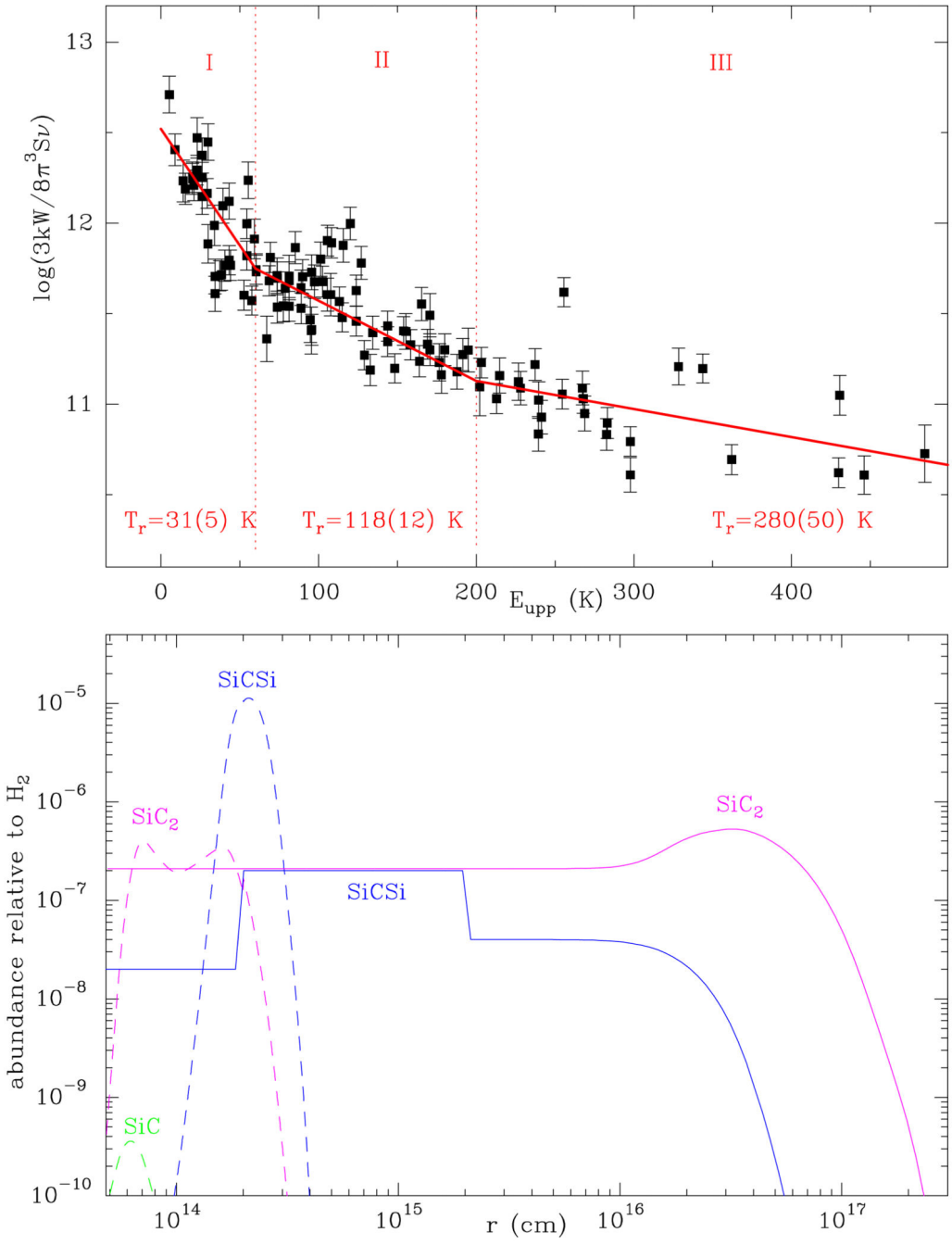

Fig. 3.

The top panel shows the rotational diagram of the 112 observed lines of SiCSi. The three zones discussed in the text are indicated by vertical dashed lines. The bottom panel shows the radial abundance distribution of SiCSi, SiC_2, and SiC as calculated by chemical equilibrium (dashed lines) and as derived from the observations of IRC +10216 (solid lines). The derived abundance profile of SiC_2 is taken from Cernicharo et al. (2010).

Europe PMC Funders Author Manuscripts

Table 1

Spectroscopic constants (MHz) of SiCSi in comparison to SiC_2

Constant	S-reduction	A-Reduction	SiC_2 A-reduction
A	64074.3366(44)	64074.33623(37)	52474.1930(677)
B	4395.51772(41)	4395.621072(844)	13158.71537(204)
C	4102.13098(62)	4102.02789(107)	10441.58029(168)
$\Delta_J \times 10^3$	9.66776(224)	9.73150(178)	13.20278(397)
Δ_{JK}	−0.856833(73)	−0.8572075(610)	1.5382238(882)
Δ_K	23.58788(178)	23.58805(148)	−1.2159(174)
$d_1/\delta_J \times 10^3$	−1.52630(34)	1.519832(437)	2.41191(253)
$d_2/\delta_K \times 10^2$	−0.00318(32)	5.1591(454)	8.70880(415)
$H_J \times 10^8$	−3.627(116)	−4.1349(949)	−8.312(460)
$H_{JK} \times 10^5$	1.9373(67)	1.93298(547)	−5.0158(993)
$H_{KJ} \times 10^3$	−1.8882(95)	−1.88755(791)	0.39025(399)
$H_K \times 10^2$	4.8632(204)	4.8633(168)	0.2487(529)
$h_1/h_J \times 10^9$	−5.304(225)	−5.231(187)	−3.46(271)
$h_2/h_{JK} \times 10^9$	−2.614(255)	−6586(361)	−35151(191)
$h_3/h_K \times 10^3$			1.1162(286)

Note. — 1 σ uncertainties (in parentheses) are in the units of the last significant digits.

Table 2

Observed lines of SiCSi in the laboratory and in IRC +10216

$(J$	K_a	$K_c)_u$	$(J$	K_a	$K_c)_l$	ν_{obs}(unc) MHz	$\int T_A^* \times dv$ K kms^{-1}	Predicted$_{Lab+Astro}$(unc) MHz	E_{upp} K	S_{ul}	σ mK
5	1	5	6	0	6	6718.9927(0.002)		6718.994 (0.001)	8.9	2.586	lab
8	0	8	7	1	7	12018.3548 (0.002)		12018.353 (0.001)	14.7	3.692	lab
20	1	19	19	2	18	19095.4772 (0.002)		19095.477 (0.002)	89.8	4.991	lab
15	2	14	16	1	15	24506.4805 (0.002)		24506.481 (0.002)	60.4	3.644	lab
3	1	3	4	0	4	24959.6919(0.002)		24959.692 (0.001)	5.3	1.528	lab
10	0	10	9	1	9	31198.7591 (0.002)		31198.761 (0.002)	22.4	4.861	lab
1	1	1	2	0	2	42663.0910(0.002)		42663.088 (0.002)	3.3	0.504	lab
2	1	1	2	0	2	60248.2200 (0.020)		60248.209 (0.003)	4.1	2.493	lab
4	1	3	4	0	4	61298.7200(0.020)		61298.746 (0.003)	7.0	4.450	lab
6	1	5	6	0	6	62974.9200 (0.020)		62974.923 (0.005)	11.6	6.340	lab
8	1	7	8	0	8	65310.0300(0.020)		65310.040 (0.008)	17.8	8.135	lab
1	1	1	0	0	0	68154.6000(0.020)		68154.606 (0.004)	3.3	1.000	lab
10	1	9	10	0	10	68348.4600 (0.020)		68348.474(0.011)	25.7	9.806	lab
3	1	3	2	0	2	84424.5800 (0.020)		84424.602 (0.006)	5.3	2.002	lab
5	1	5	4	0	4	100120.6600(0.040)		100120.678 (0.009)	8.9	3.022	lab
8	2	6	9	1	9	109709.6000(0.040)		109709.645 (0.018)	26.2	1.447	lab
7	1	7	6	0	6	115262.8500(0.040)		115262.899 (0.013)	14.1	4.073	lab
11	1	11	10	0	10	144033.4200(0.040)		144033.475 (0.023)	29.3	6.327	lab
3	2	2	3	1	3	180036.9000(0.040)		180036.916 (0.017)	13.9	1.456	lab
5	2	4	5	1	5	181405.4500(0.040)		181405.432 (0.014)	17.6	2.548	lab
7	2	6	7	1	7	183384.5800(0.040)		183384.603 (0.012)	22.9	3.561	lab
9	2	8	9	1	9	185976.7800(0.040)		185976.772 (0.012)	29.8	4.527	lab
16	1	15	16	0	16	82260.5000 (0.500)	0.109 (22)	82260.891 (0.029)	59.2	13.826	1.7
3	1	3	2	0	2	84424.1900(0.330)	0.107 (18)	84424.602 (0.005)	5.3	2.002	1.4
9	2	8	10	1	9	86429.8400 (0.500)	0.059 (10)	86429.537 (0.008)	29.8	1.888	1.1
18	1	17	18	0	18	88716.0400(1.150)	0.091 (14)	88715.413 (0.040)	73.7	14.774	1.7

Note. — 1 σ uncertainties (in parentheses) are in the units of the last significant digits. The full table containing all observed lines can be found in the online version of the paper.